ACS Photonics

pubs.acs.org/journal/apchd5

Article

Nanoparticle Trapping in a Quasi-BIC System

Sen Yang, Chuchuan Hong, Yuxi Jiang, and Justus C. Ndukaife*

Cite This: *ACS Photonics* 2021, 8, 1961−1971

Read Online

ACCESS | Metrics & More | Article Recommendations | Supporting Information

ABSTRACT: Plasmonic nanotweezers employing metallic nanoantennas provide a powerful tool for trapping nanoscale particles, but the strong heating effect resulting from light absorption limits widespread applications. Here, we propose an all-dielectric nanotweezer harnessing quasi-bound states in the continuum (quasi-BICs) to enable the trapping of nanoscale objects with low laser power and a negligible heating effect. The quasi-BIC system provides very high electromagnetic field intensity enhancement that is an order of magnitude higher than plasmonic systems as well as high-quality-factor resonances comparable to photonic crystal cavities. Furthermore, the quasi-BIC metasurface tweezer array provides multiple optical hotspots with high field confinement and enhancement, thereby generating multiple trapping sites for the high-throughput trapping of nanometer-scale objects. By purposefully truncating the tips of the constituent elliptical nanoantennas in the quasi-BIC system to leverage the asymmetric field distribution, we demonstrate that the optical gradient forces can be further enhanced by a factor of 1.32 in comparison to the intact elliptical nanoantenna, which has attractive potential in subwavelength particle trapping applications. In addition, we show that trapped particles can improve the resonance mode of the cavity rather than suppress it in a symmetry-broken system, which in turn enhances the trapping process. Our study paves the way for applying quasi-BIC systems to low-power particle trapping and sensing applications and provides a new mechanism to harness the self-induced back-action.

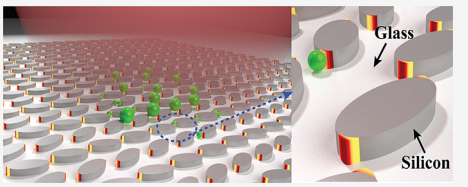

KEYWORDS: *all-dielectric metasurface, bound states in the continuum, optical trapping, self-induced back-action, electric field enhancement, nanophotonic cavity*

Optical trapping technology has found many applications in biology and medicine[1−5] and colloidal assembly[6,7] because it provides precise control and noninvasive manipulation of microscale particles. For example, the traditional optical tweezer has been utilized to manipulate microscale objects such as bacteria, colloidal particles, and cells[8−10] and was recently recognized with a 2018 Nobel Prize in physics awarded to Arthur Ashkin for his pioneering work on optical tweezers.[11] The single-beam optical tweezers demonstrated in 1986[8] utilizes a tightly focused laser beam to trap particles near the focal spot of the laser. Due to the diffraction limit of light that precludes the focusing of light to nanoscale subwavelength volumes, the low-power trapping of nanoscale objects by optical tweezers is challenging. Plasmonic nanotweezers[12] have generated significant interest because plasmonic nanoantennas can confine light to nanoscale volumes with high field enhancement. Such subwavelength hotspots generate the tight trapping potential wells required to trap nanoscale objects. Different kinds of plasmonic nanoantenna geometries have been explored including nanoholes,[13−16] coaxial apertures,[17,18] double-nanoholes,[19−21] nanopillars,[22] dimers,[23] bowties,[24,25] and bowtie apertures.[26] Although plasmonic nanotweezers have been proven to be effective for trapping subwavelength nanoparticles by overcoming the diffraction limit, the photoinduced heating effect resulting from the intrinsic loss of the metallic materials generates undesired thermal effects such as thermophoresis and convection,[12,27] and the excessive temperature rise can damage trapped particles especially biological objects such as cells. In addition, it is imperative to note that many of the previously reported near-field optical nanotweezers typically possess one or a few hotspots that define the trapping potential where the target objects in the solution can be trapped. A platform that possesses multiple hotspots is crucial for achieving the multiplexed manipulation of multiple nanoscale objects. Although some works have demonstrated multiple nanoparticle trapping,[28−31] this field presents many possibilities. Here we propose to realize these new features by harnessing an all-dielectric metasurface supporting supercavity resonances enabled by bound-states-in-the-continuum. A metasurface[32−34] is an artificial nanostructured interface with a subwavelength thickness that manipulates light by spatially arranged nanoantennas. It has found many applications in wavefront shaping,[35−37] waveguides,[38] fibers,[39,40] and flat lenses.[41,42] Recently, bound states in the continuum (BICs), which were first proposed in quantum mechanics[43] and refers to a kind of nonradiating states of light in photonics, have attracted

Received: December 22, 2020
Published: June 21, 2021

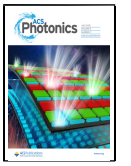

https://doi.org/10.1021/acsphotonics.0c01941
ACS Photonics 2021, 8, 1961−1971

extensive attention in photonics due to the ability to achieve high-quality-factor (Q factor) resonances as well as high field enhancement. An ideal BIC has no out-coupling. As a result, the Q factor of the mode is infinite, and it cannot be observed in the spectrum. True BICs cannot be realized in practice due to fabrication imperfections and material loss.[44,45] If the outgoing radiation is not totally vanishing, a sharp peak can then be observed in the spectrum, and the Q factor does not go to infinity. Such a case is called a quasi-BIC. Many applications of quasi-BICs have been reported to date, including biosensing,[46−48] nonlinear optics,[49−51] chiral sensing,[52] unidirectional radiation,[53] and lasers.[54] In this paper, we specifically focus on the symmetry-protected BIC,[55−57] which is one class of BICs and appears when the spatial symmetry of the mode is incompatible with the symmetry of the outgoing radiating channels. Symmetry-protected quasi-BICs have been demonstrated in a variety of photonic structures such as metasurfaces,[46,56] photonic crystal slabs,[58] and waveguide arrays.[59]

The quasi-BIC system can provide very high field enhancement comparable to or even higher than in plasmonic systems. Additionally, the quasi-BIC system also provides much higher field enhancements than the levels achievable in Mie resonant dielectric nanoantenna systems[60] with no need for a critical geometry.[24,26] Moreover, in contrast to plasmonic nanostructures, the quasi-BIC system also has a very high Q factor (10^2−10^6), comparable to photonic crystals (PhC), making it a good candidate for trapping-assisted sensing applications. Additionally, the dielectric quasi-BIC system has almost no material absorption and thus negligible heating effects. This feature is especially critical for nano-optical trapping of biological specimens without detrimental photoinduced heating effects present in plasmonic systems. On the other hand, in comparison with a typical PhC cavity system,[61] the quasi-BIC system has much higher field confinement, although some recent works have reported the realization of deep-subwavelength confinement by unique designs of PhC cavity geometries.[62,63]

We also present a new mechanism for harnessing the self-induced back-action (SIBA) effect based on the proposed quasi-BIC system. The SIBA effect first proposed using a plasmonic gold nanohole structure[16,64] is a powerful technique for enhancing optical trapping under low optical intensities, reducing the power required for stable trapping by 1 order of magnitude. In the particle−cavity system, the trapped particle itself perturbs the local electric field and thus plays an active role in the dynamics of the trapping process. To be specific, when a particle moves away from its equilibrium position, by virtue of Newton's law, the momentum exchange between the photons and the particle induces a back-action force that pulls the particle back toward the cavity. The SIBA effect has been shown to exist in some nanophotonic systems such as plasmonic nanoantennas[19,26,65−67] and photonic crystals.[68,69] However, the previous works[67,69,70] have only analyzed the resonance frequency shift induced by the perturbation of particles to the cavity. How the trapped particles alter the resonance mode (the quality factor of the mode, for example) remains unclear. To reveal this mechanism, we need a system that meets three fundamental conditions: high quality factor (Q factor), high field enhancement, and high sensitivity to perturbations. Traditional plasmonic nanostructures can fulfill the latter two requirements but usually have a low Q factor. The proposed quasi-BIC system supports these features, which provides a novel platform to investigate the SIBA effect from a new perspective.

In this paper, we systematically discuss the optical trapping process in a dielectric quasi-BIC system for the first time (as shown in Figure 1). The organization of this paper is as follows. First, we study the optical trapping in a symmetry-protected quasi-BIC system composed of pairs of complete elliptical dielectric nanoantenna elements and present its features, including high field enhancement, high quality factor, negligible heating effect, and multiple hotspots, which make it suitable for particle-trapping applications. By purposefully breaking the symmetry of the trapping gaps where the two tips on one end of the nanoantenna elements in each unit cell are truncated, we demonstrate that the trapping force and stability can be further improved via the doubly truncated quasi-BIC system. The robustness of the system to fabrication uncertainties and the characterization of its trapping performances are then investigated. Owing to the high Q factor, high field enhancement, and high sensitivity to perturbations of this quasi-BIC system, we also investigate the relationship between the trapped particles and the cavity resonance mode. Our analysis reveals that particles trapped in the original intact elliptical dielectric nanoantenna array will break the system's symmetry and slightly suppress the resonance mode of the cavity. We consider truncating only one tip of the nanoantenna elements in each unit cell to address this effect. Then, we present an idealized scenario, where we show the positive influence of the trapped particles on the resonant modes of the quasi-BIC system. The trapped particles partially compensate for the truncated part and improve the resonance performance of the symmetry-breaking quasi-BIC system. This in turn results in an increased Q factor and peak reflectance as well as stronger optical trapping forces. Both numerical and analytical investigations are presented to elaborate on this concept.

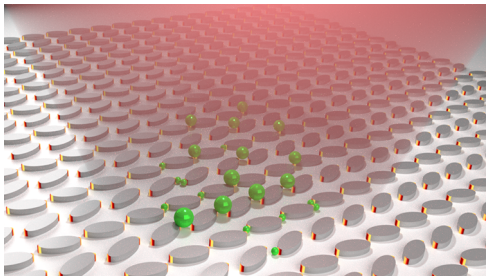

Figure 1. Schematic diagram for the quasi-BIC metasurface. Gradient colors at the tips show the field enhancement distribution.

Optical Trapping in the Quasi-BIC System. We start from the symmetry-protected quasi-BIC metasurface based on complete elliptical nanoantennas.[46,56] As shown in Figure 2a, a unit cell is composed of two silicon elliptical resonators with a tilt angle of ±5°. The detailed geometrical parameters are given in the caption of Figure 2. Our design is tuned to work in the C band of the optical communication wavelength bands, and the resonator side is immersed in water for particle-trapping purposes.

To understand the generation of the quasi-BIC mode, we consider the two inverse electric dipoles (black arrows in Figure 2b) excited in the two resonators by an incident x-polarized light. Each electric dipole is decomposed into two directions, i.e., p_x and p_y in Figure 2b. Although p_y is dominant in each resonator, the directions of the p_y components are

https://doi.org/10.1021/acsphotonics.0c01941
ACS Photonics 2021, 8, 1961−1971

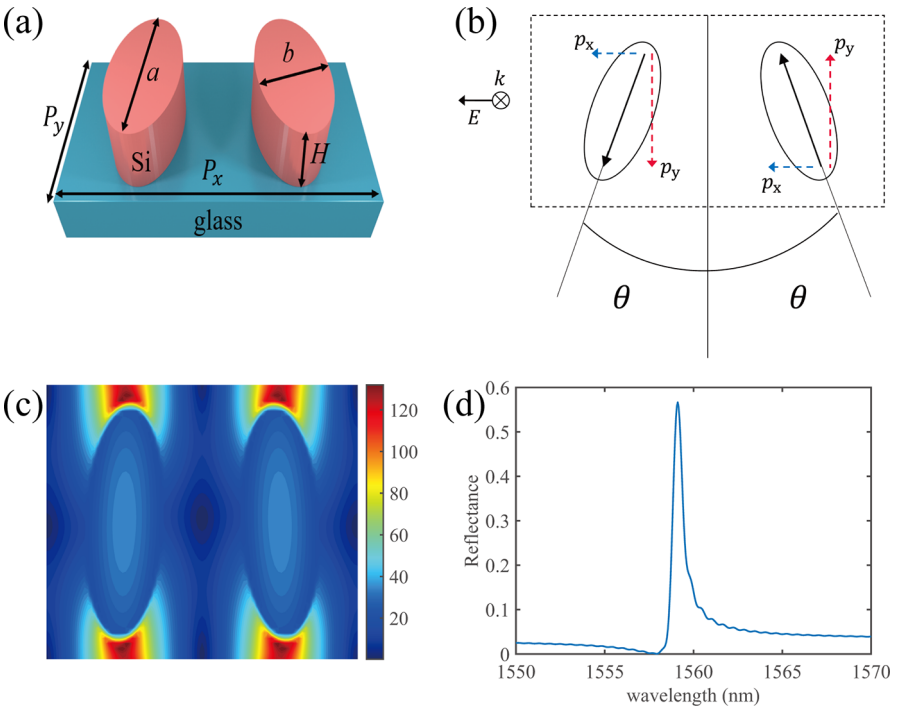

Figure 2. (a) Schematic diagram of a unit cell of the symmetry-protected quasi-BIC metasurface. Geometrical parameters are P_x = 894 nm, P_y = 515 nm, a = 445 nm, b = 216 nm, H = 175 nm, and θ = 5°.The resonator side is surrounded by water. The refractive indexes are extracted from the *Palik* database in Lumerical (see Methods for details). (b) Diagram depicting the electric dipoles induced in the two resonators. The incident light is linearly polarized light with polarization perpendicular to the mirror plane (yz plane in this figure). The blue and red dashed arrows represent the two dipole components p_x and p_y, respectively. (c) Electric field enhancement distribution of the xy plane ($z = H/2$) for one unit cell. The maximum field enhancement is 141, which is defined as the maximum electric field enhancement factor on the xy plane when $z = H/2$. The electric field is confined in the gaps, reflecting a collective effect. (d) Reflection spectrum for an infinite array. The reflectance peak is 56.6% due to water absorption in this wavelength band.

inverse for the two resonators, which cancel with each other, and thus the out-coupling of p_y is forbidden. When the tilt angle θ is small, the overall radiative loss is suppressed significantly. Hence, a fairly narrow reflection peak, as well as a high field enhancement, can be obtained. Since the Q factor of this system satisfies[46,56] $Q \propto \sin^{-2}\theta$ and we have selected a small tilt angle of θ = 5°, the electric field enhancement is extremely high (∼141) at the tips of each resonator, as shown in Figure 2c. Therefore, water absorption cannot be neglected even though it is relatively small (n = 1.31 + 0.00013i at λ = 1550 nm). This additional lossy channel perturbs the quasi-BIC mode, and the reflectance is reduced to 56.6% instead of approximately 100% reported in the previous work.[46] The reflection spectrum is shown in Figure 2d, where the line width is 0.65 nm, and the corresponding Q factor is 1940.

The high field enhancement in our design, which is also spatially confined, provides a key advantage for optical trapping applications. Figure 3a shows the electric field distribution of two unit cells when a silicon sphere is trapped in one gap. Here we define a parameter "trapping density" σ = 1/2, which means every two unit cells share one trapped particle in the infinite array. Due to the high index contrast between the sphere and the medium, a much higher field enhancement is observed near the sphere's surface. Figure 3b shows the force spectra of the silicon sphere depicted in Figure 3a. Figure 3c and d show the temperature fields when a 30 μm by 30 μm nanoantenna array on the glass substrate is excited at resonance. The negligible temperature rise (less than 0.01 K) confirms the low heating effect from our design. This is because most heat dissipation comes from water absorption instead of the resonators.

Since the optical gradient force is proportional to the gradient of the square of the local electric field $F_{grad} \propto \nabla |\vec{E}(r)|^2$, we next investigate a truncated quasi-BIC system, wherein the trapping stability can be further improved by leveraging the asymmetry introduced in the gap. To demonstrate this, we purposefully truncate out a small part of both tips of the resonators in each unit cell to break the symmetry of the original system (see Figure 4a). We refer to this as the "2 cuts" system, and for the original system in Figure 2a we refer to it as the "0 cuts" system. For comparison with the "0 cuts" system, we have adjusted the gap size of the "2 cuts" system to have the same gap size as the "0 cuts" system. The tip-to-tip gap size for both the "0 cuts" and "2 cuts" system is approximately 70 nm. Figure 4a shows the electric field distribution of two unit cells of the "2 cuts" system that presents approximately the same maximum field enhancement compared with the original "0 cuts" system. The inset shows a higher field enhancement at the intact tip (the black dashed ellipse) compared with the truncated tip (the white dashed ellipse) due to the larger curvature of the intact tip, which can induce a larger gradient force on the particle trapped in the gap. As shown in Figure 4b, the "2 cuts" system shows approximately the same peak reflectance value compared with the original "0 cuts" system. The force spectra of silicon spheres with the same size and relative position in the "2 cuts" and "0 cuts" systems are shown in Figure 4c. It can be found that the peak value of F_y on the sphere (66.10 pN/mW)

https://doi.org/10.1021/acsphotonics.0c01941
ACS Photonics 2021, 8, 1961−1971

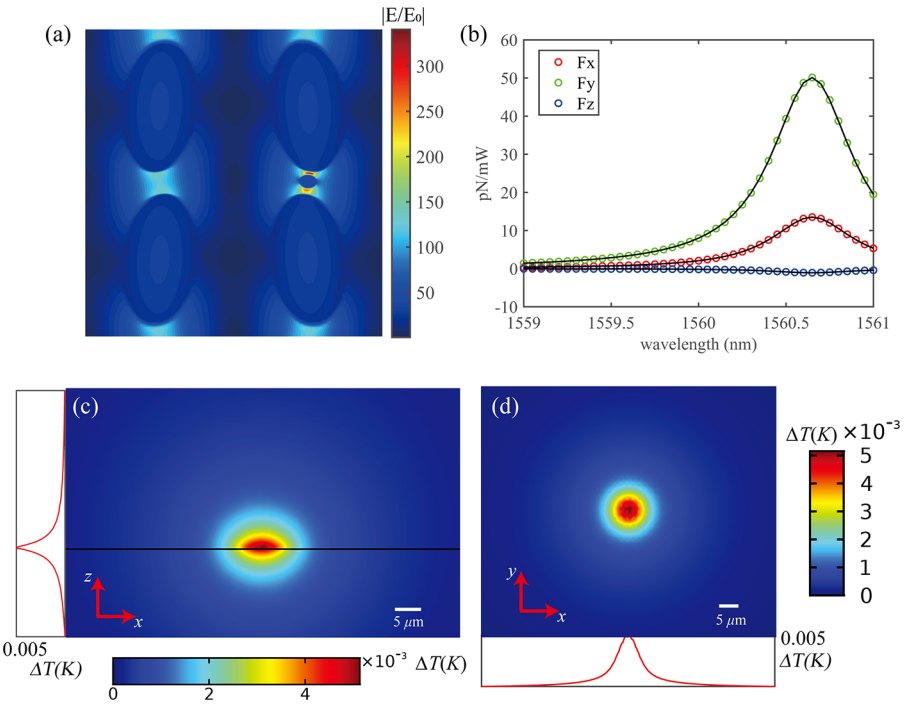

Figure 3. (a) Electric field enhancement distribution for $\sigma = 1/2$. The diameter of the trapped silicon sphere is $D = 50$ nm. The maximum field enhancement is 347. To describe the position of the sphere, we define $x_0 = P_x/4$, $y_0 = P_y/2$, $z_0 = H/2$. The center position of the left bottom resonator can be expressed as $x = -x_0$, $y = -y_0$, $z = z_0$. Therefore, the center position of the sphere in (a) is described as $x = x_0$, $y = 5$ nm, $z = z_0$. We will follow the coordinate notations here in this paper. This set of geometrical parameters is applied to all systems (except for the second section) for comparisons between different systems. (b) Force spectra for the silicon spheres depicted in (a). Temperature fields of the (c) xz plane and (d) xy plane for a 30 μm by 30 μm quasi-BIC array on the glass substrate. The maximum temperature rise is 0.005 K.

trapped in the gap of the "2 cuts" system is larger (by 1.32 times) than that of the same sphere trapped in the original "0 cuts" system (50.12 pN/mW), validating the improvement on trapping stiffness in the xy plane. This enhancement in the trapping forces for the "2 cuts" system relative to the "0 cuts" system is because truncating the tip of the antenna on one end results in an increased gradient of the electric field in the gap in comparison to the untruncated ("0 cuts") system. The comparison of the profiles of $\partial|\vec{E}(r)|^2/\partial y$ between the "0 cuts" and the "2 cuts" system is shown in Figure S6. Since the optical gradient force in the quasistatic limit is proportional to the gradient in the electric field, the "2 cuts" system with the enhanced electric field gradient generates an increased optical gradient trapping force. We have also investigated the impact of fabrication imperfections on the quality factor of the quasi-BIC antenna system. We have fabricated the "2 cuts" system and compared it with the designed system from numerical simulations. Figure 4d shows the SEM image of a fabricated antenna array. The tilt angle has been set to $\theta = 15°$ because this is easier to fabricate using the readily available nanofabrication facility. As shown in Figure 4e, by inputting two unit cells of the SEM images into the numerical simulation model, the fabricated array presents a similar reflection spectrum compared to the designed array with only a slight red-shift.

Subsequently, we have simulated the performances of the "2 cuts" system for practical optical trapping applications of relevant nanoscale particles, as depicted in Figure 5. Figure 5a shows the force spectra for some small particles comprising exosomes, quantum dots, and bovine serum albumin (BSA) protein molecules. Their hydrodynamic diameters are taken as 30, 20, and 5 nm, respectively. Although the quantum dots are smaller than exosomes, they show larger forces due to their larger refractive index of 2.49 relative to that of the exosomes ($n = 1.38$) and the water medium ($n = 1.31$). Since the forces are normalized, the results show that stable trapping for these particles is expected even under lower laser power of a milliwatt. Figure 5c shows the trapping potential of a 30 nm polystyrene (PS) sphere located above the top surface of the resonators and moving along the path depicted by the red arrow in the inset. A broad and deep potential well is observed within the gap of the "2 cuts" system. The depth of the potential well is larger than 10 k_BT/mW, which is sufficient to trap the PS sphere stably in the xy plane. The corresponding optical forces with respect to the sphere's positions along the y direction are shown in Figure 5b. Figure 5d shows the optical trapping potentials for the same PS sphere trapped in the original "0 cuts" system and the "2 cuts" system along the z direction obtained by evaluating the integral[73] $U(\mathbf{r}_0) = \int_{\infty}^{r_0}\mathbf{F}(\mathbf{r})\cdot d\mathbf{r}$. It can be noticed that the middle height z_0 (the left black dashed line) is the equilibrium position with $F_z = 0$, which corresponds to the bottom of the trapping potential well. Near the top surface level $z = H$ (the right black dashed line), the steep slope of the potential curve indicates a strong force pulling the particle back toward the gap. The broad potential well indicates that the confinement in the z direction experienced by a trapped particle is not strong, while the large depth of the potential well (~59 k_BT/mW) guarantees a strong back force pulling the particle back when it reaches the top surface. Moreover, the "2 cuts" system presents a deeper trapping potential well along the z direction than the original "0 cuts" system, indicating improved trapping stability along the longitudinal direction. These properties make the "2 cuts"

https://doi.org/10.1021/acsphotonics.0c01941
ACS Photonics 2021, 8, 1961−1971

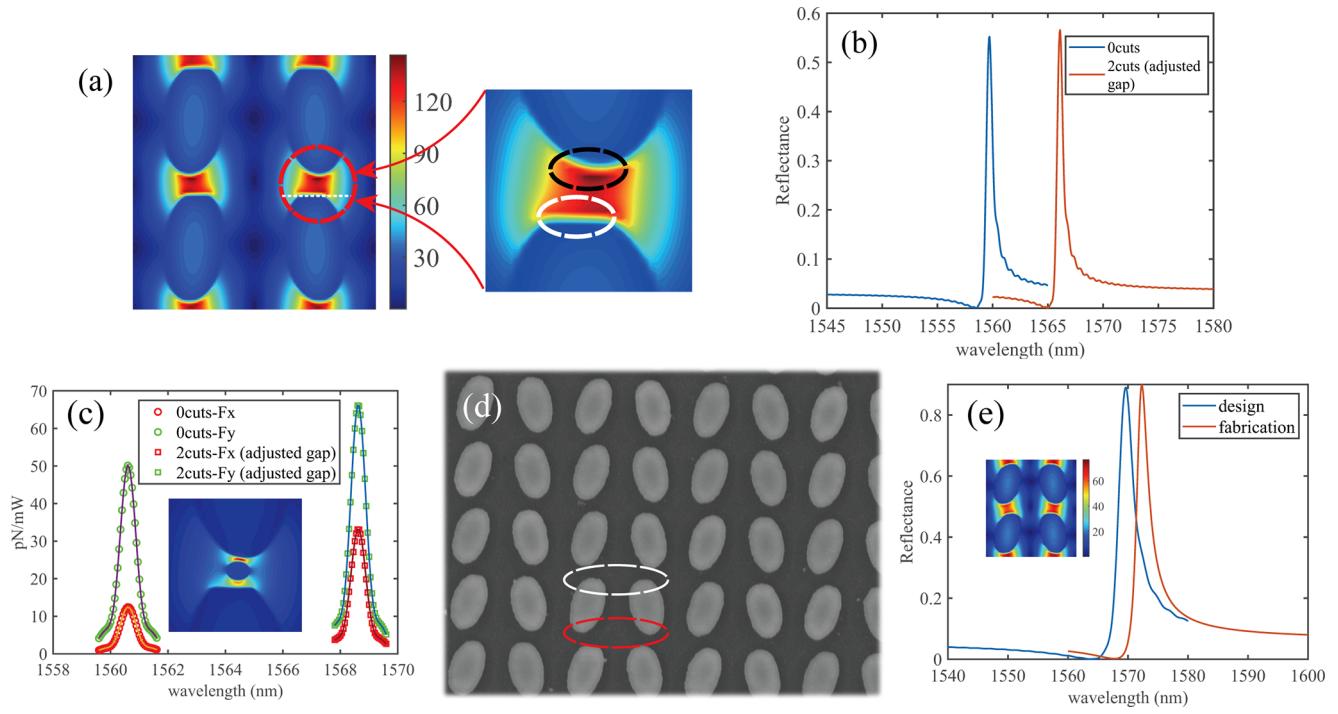

Figure 4. (a) Electric field enhancement distribution for the "2 cuts" system with adjusted gap size. The tip-to-tip gap size is approximately 70 nm in both "0 cuts" and "2 cuts" systems. Here we set $P_y = P_{y0} - 20$ nm = 495 nm for the "2 cuts" system to keep the symmetry while adjusting the gap size. Following the coordinates notation described above, the tip is vertically truncated along the z direction, and the line equation of the edge (labeled by the white dashed line) is $y = -45.5$ nm. All other geometrical parameters of the resonators are the same. The maximum field enhancement is 147. Inset: Zoom-in figure showing the field enhancement difference between the two tips. (b) Reflection spectrum for the original "0 cuts" and the "2 cuts" system. (c) Force spectra of the same silicon spheres trapped in the "0 cuts" system and the "2 cuts" system with $\sigma = 1/2$. The relative position of the sphere in the gap is approximately the same as in the "0 cuts" and the "2 cuts" system for comparison. Inset: Zoom-in figure shows the field enhancement difference for the "2 cuts" system with $\sigma = 1/2$, which induces a larger gradient force. (d) SEM image of the fabricated "2 cuts" array. The tilt angle is designed as $\theta = 15°$. The white dashed ellipse labels two truncated tips, while the red dashed ellipse labels two intact tips. (e) Reflection spectra for the designed and fabricated "2 cuts" array calculated by FDTD Solutions. The tilt angle is $\theta = 15°$. Inset: Electric field enhancement distribution for the fabricated "2 cuts" array. Notice that the field enhancement is lower for $\theta = 15°$ in comparison to $\theta = 5°$. The model for the fabricated array in FDTD Solutions is built from the SEM image in (d).

system an ideal platform for nanoscale particle-trapping applications.

SIBA Effect with Truncated Quasi-BIC Antenna System. As we have mentioned previously, to the best of our knowledge, discussions on how trapped particles alter the resonance performance of the cavity rather than the resonance frequency have not been reported so far. This section investigates the relationship between the cavity resonance and trapped particles and presents a new mechanism to generate the SIBA effect based on this quasi-BIC antenna system. Our discussions are based on an idealized scenario assuming an infinite array where trapped particles are periodically placed in the gaps.

To begin the discussion, we refer to the "0 cuts" system where the tips are intact and investigate the influence of the trapping density on the resonance performance. For demonstrating this concept, we make the assumption for the following section that trapped spheres are always placed in the right-side gap in each unit cell for all the trapping density values. The placement of particles for $\sigma = 2/3$ in the "0 cuts" system is intuitively depicted via the electric field enhancement distribution shown in Figure 6a. Due to the high Q factor, perturbation to the "0 cuts" system by trapped silicon spheres cannot be neglected, and a red-shift when increasing the trapping density is observed (seen in Figure 6b). It should be noted that the reflectance of the system is also decreasing with increasing trapping density. This means that the quasi-BIC mode is slightly suppressed, and the scattering loss increases when a particle gets trapped in the gap. To verify that the quasi-BIC mode is suppressed in the "0 cuts" system, we have fitted the reflection spectrum to a Fano line shape to extract the Q factor for different σ (see Methods for details), as shown in Figure 6c. Both the Q factor and the field enhancement show a drop with a higher trapping density. A qualitative explanation is that the extra dipole moment excited in the silicon sphere breaks the original symmetry of the system. In other words, the p_y components of the left and right resonators are not able to equally cancel with each other due to the extra dipole moments provided by the trapped particles.

We next consider a "1 cut" system where particles are trapped in the truncated region (see the inset of Figures 7a and S1). In contrast to a negative impact on the quasi-BIC mode, particles trapped in the asymmetric gap of the "1 cut" system instead play a positive role in enhancing the performance of the mode. Direct evidence can be found from the reflectance spectrum shown in Figure 7a, where the peak reflectance increases with increasing the trapping density σ. When no particles are trapped (i.e., $\sigma = 0$), the reflectance decreases dramatically from 56.6% in the "0 cuts" system to 46.0%, attributed to breaking the symmetry, while the reflectance increases again with increasing σ, in contrast to the trend of the "0 cuts" system where the reflectance decreases with increasing

https://doi.org/10.1021/acsphotonics.0c01941
ACS Photonics 2021, 8, 1961−1971

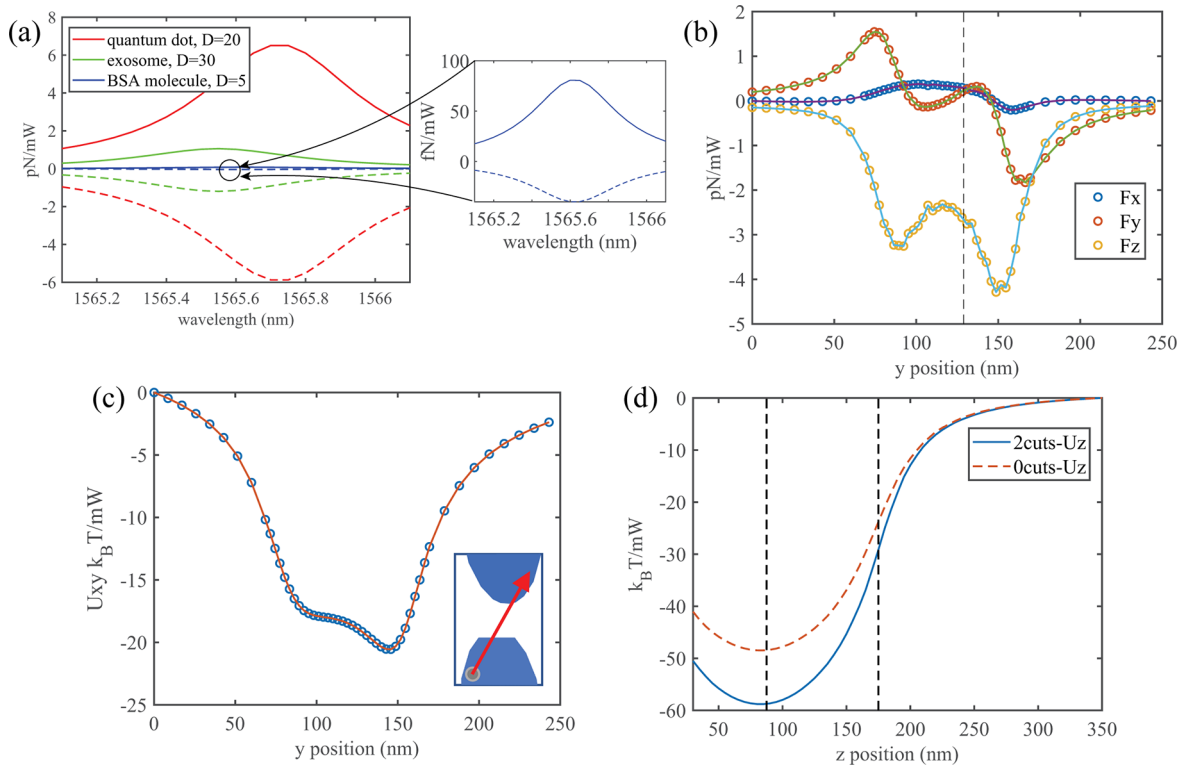

Figure 5. (a) Force spectra for small particles, including exosomes, quantum dots, and BSA molecules. The geometrical parameters are $\sigma = 1/2$, $x = x_0$, $z = H$, $y = 8$ nm, $y = 12$ nm, and $y = 23$ nm for exosomes, quantum dots, and BSA molecules, respectively. The refractive index for each particle, namely, exosomes, quantum dots, and BSA, is 1.38, 2.49,[74] and 1.45,[75] respectively. D in the legend denotes the diameter of each particle. Solid lines correspond to F_y, while dashed lines correspond to F_z. Inset shows a zoom-in view of the force spectra for BSA molecules. (b) Trapping forces corresponding to the trapping potential in (c). The vertical black dashed line indicates the center of the gap (i.e., close to the equilibrium position in the xy plane). The "y position" in both (b) and (c) is the y coordinates relative to the starting position. (c) Trapping potential of a PS sphere ($n_{PS} = 1.59$, $D = 30$ nm) moving along the red arrow 5 nm above the top surface of the resonators. A broad and deep potential well is observed, corresponding to the gap region. Inset depicts the trajectory of the sphere. (d) Optical trapping potential wells for the "0 cuts" and "2 cuts" systems when moving a PS sphere along the z direction in the gap. The two vertical black dashed lines correspond to $z = z_0$ and $z = H$, respectively. The trajectory of the sphere center is $z = 30$ nm to $z = 2H$. The geometrical parameters are $D = 30$ nm, $\sigma = 1/2$, $x = x_0$, and $y = 0$ (center of the gap for comparison). The laser wavelength is set as the resonance wavelength when the sphere center is at $z = z_0$ in each case.

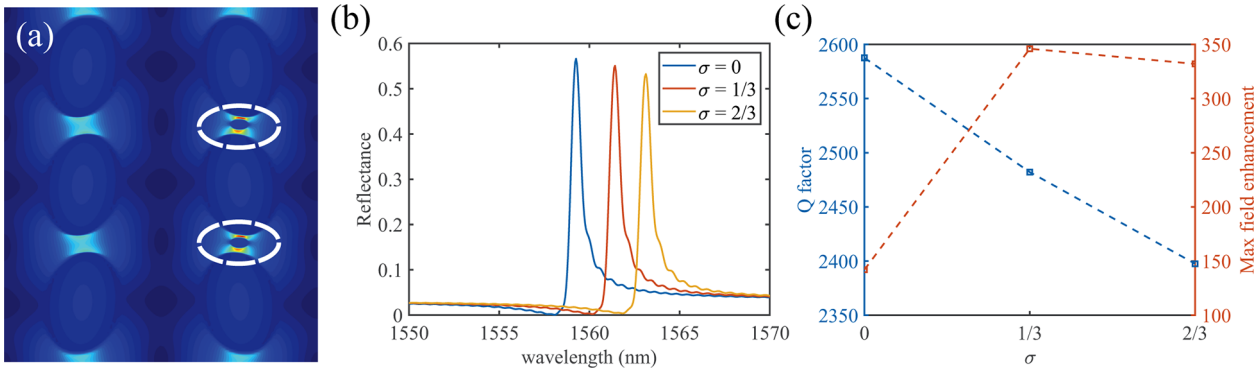

Figure 6. (a) Electric field enhancement distribution for $\sigma = 2/3$ depicting the placement of particles. White dashed ellipses show the placement of the spheres. The positions of the silicon spheres are $x = x_0$, $y = 5$ nm, and $y = 5$ nm + P_y, respectively. (b) Reflection spectra for different trapping densities $\sigma = 0$, 1/3, and 2/3. With a higher trapping density, the resonance wavelength shows a red-shift, and the peak reflectance decreases. (c) Q factor and maximum field enhancement with respect to the trapping density. The Q factor is decreasing, denoting a suppression of the quasi-BIC mode by trapped particles. The maximum field enhancement jumps up when the trapping density is not zero, originating from the high index contrast between silicon and water. It then gradually decreases due to the perturbation of trapped particles.

σ (see Figure 6b). The new dipole moment induced in the trapped silicon sphere partially compensates for the lost part of the truncated resonator and hence enhances the quasi-BIC mode. In other words, the effective index in the gap gets increased and becomes closer to that in the original system. By multipole decomposition analysis[71] shown in Figure 7b, we can find that the electric dipole around the right antenna is increased after trapping a particle, consistent with our expectation. To further prove this positive effect, the Q factors and the maximum field enhancements with respect to the

https://doi.org/10.1021/acsphotonics.0c01941
ACS Photonics 2021, 8, 1961−1971

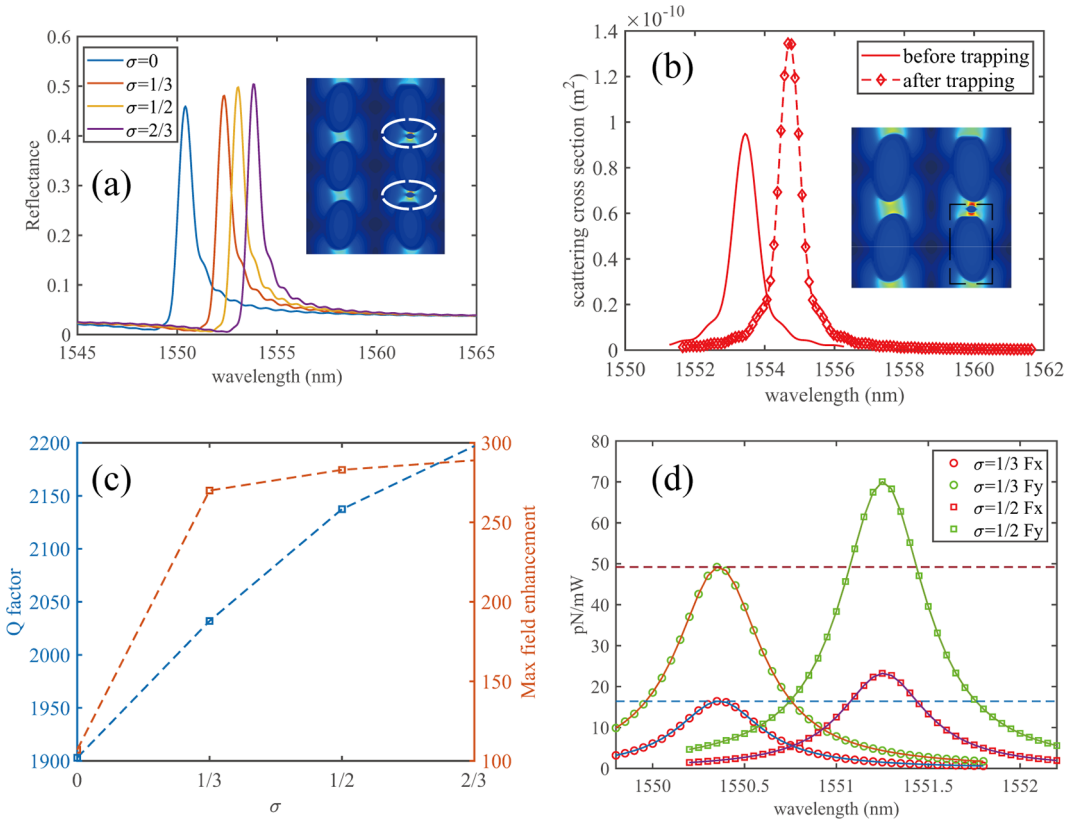

Figure 7. (a) Reflection spectra for different trapping densities in the "1 cut" system: σ = 0, 1/3, 1/2, and 2/3. Similar to the "2 cuts" system, the line equation of the truncated edge is expressed as $y = -55.5$ nm. All other geometrical parameters are the same as the original "0 cuts" system (i.e., the gap size is not adjusted). With a higher σ, the resonance wavelength shows a red-shift and the peak reflectance is increased. Inset: Electric field enhancement distribution for σ = 2/3 depicting the placement of particles. White dashed ellipses show the placement of the spheres. (b) Multipole decomposition analysis showing the electric dipole components before (solid line) and after (dashed line with diamonds labeling data points) a silicon sphere is trapped with σ = 1/2. An increase can be seen after a particle is in the gap, indicating the compensation for the lost part of the resonator. For other multipole curves, refer to Figure S5 for details. Inset shows the region (the black dashed rectangle) where the multipole decomposition analysis is applied. (c) Q factor and maximum field enhancement both increase with increasing σ, denoting a positive perturbation, in contrast to particles trapped in the original system (seen in Figure 6c). (d) Force spectra of silicon spheres trapped in the "1 cut" system with σ = 1/3 and σ = 1/2, respectively. The peak values of forces are F_x = 16.43 pN/mW, F_y = 49.21 pN/mW for σ = 1/3 and F_x = 23.23 pN/mW, F_y = 70.05 pN/mW for σ = 1/2, respectively. The two horizontal dashed lines denote the peak values of forces when σ = 1/3.

trapping density are shown in Figure 7c. It is evident that the Q factors and maximum field enhancement both increase with increasing σ, which is opposite the trend of the "0 cuts" system (see Figure 6c). Since both a higher Q factor and a higher field enhancement denote a higher local density of photon states, the improvement of the quasi-BIC mode is verified. The electromagnetic field distributions for different trapping densities are shown in Figure S3. This effect still occurs for low-index particles such as PS spheres (n = 1.59, see Figures S2 and S4 for details).

To qualitatively demonstrate how this particle-enhanced effect assists with the trapping process, we have derived the expression for the force F_y where the x and z components are not considered since they are much smaller in the gap. The equations of one-dimensional particle motion while only considering optical forces can be expressed as[70]

$$\frac{dy}{dt} = \frac{p}{m} \tag{1}$$

$$\frac{dp}{dt} = -n(y)\hbar\frac{d\omega_c(y)}{dy} \tag{2}$$

$$\frac{d\beta}{dt} = i(\omega_L - \omega_c(y))\beta - \frac{\kappa}{2}\beta + i\sqrt{\kappa_{ex}}E_0 \tag{3}$$

where p is the momentum of the particle, β is the expectation value of the photon amplitude, while $n = |\beta|^2$ is the expectation value of the photon number in the cavity. $\omega_c(y) = \omega_0 + \delta\omega_c(y)$ denotes the resonance frequency of the system as a function of particle position y, while ω_0 and $\delta\omega_c(y)$ describe the resonance frequency of the empty cavity and the resonance shift due to the particle perturbation, respectively. $\kappa = \kappa_{ex} + \kappa_{int} + \kappa_{scat}(y)$ is the total cavity decay rate[72] (also the total line width), and the Q factor of the empty cavity is defined as $Q = \omega_0/(\kappa_{ex} + \kappa_{int})$. Here κ_{ex} denotes the decay rate of the empty cavity into particular external channels (such as backward scattering), which also serves as the source of injection of photons into the cavity with number flux E_0^2 and frequency ω_L. κ_{int} denotes the intrinsic loss rate resulting from water and material absorption. $\kappa_{scat}(y)$ describes the scattering rate of trapped particles and is a *negative* value here in contrast to that in the previous work[70] because the presence of particles increases the Q factor (i.e., decreases the total line width). By solving eqs 1 to 3, we show that the y component of the optical forces satisfies $F_y \propto \frac{\kappa_{ex}}{\kappa}$ (see Supporting Information S1 for the detailed derivation) at the

https://doi.org/10.1021/acsphotonics.0c01941
ACS Photonics 2021, 8, 1961−1971

resonance wavelength. Here we assume that the laser wavelength can be freely tuned to reach a resonance for the particle at a specific position, which is different from the previous work,[70] where the laser wavelength ω_L is considered to be fixed. With particles trapped in the gap, the Q factor increases, namely, the total decay rate κ decreases, giving rise to an increase of F_y. The numerical evidence from the aspect of trapping density is shown in Figure 7d. When increasing the trapping density from $\sigma = 1/3$ to $\sigma = 1/2$ in the "1 cut" system, the peak values of F_x and F_y on the same sphere are increased, directly confirming the positive response of our "1 cut" system when particles are trapped. Additional proofs for such particle-assisted trapping effect can be found in the Supporting Information S3.

Since we have assumed collective placement of multiple particles, it is instructive to investigate a scenario in the limit of low particle density. For this case, we have simulated a 20 μm by 20 μm "1 cut" array and placed only five silicon spheres in the truncated regions. We find that for such low particle density, trapping of particles in the truncated region does not improve the resonance quality of the quasi-BIC mode. Figure 8

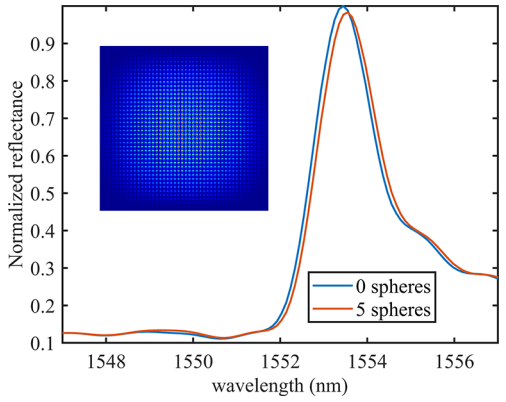

Figure 8. Normalized reflection spectra before and after five silicon spheres are trapped at the center region of a 20 μm by 20 μm "1 cut" array. A PML boundary condition is applied, and the incident light is set as a Gaussian beam with the beam waist radius of 10 μm. Inset: Electric field enhancement distribution for the whole array without particles.

shows the simulation results before and after five silicon spheres (i.e., $\sigma = 5/858$) are trapped at the center region of a 20 μm by 20 μm "1 cut" array illuminated by a Gaussian beam. The reflection spectra present a slight red-shift, while the differences between the reflectance peak values are small enough to be considered as numerical calculation tolerance. On the basis of our findings, we predict that the trapping stability would increase when more particles are trapped in the asymmetric gap, while no enhancement in the trapping stability is expected for low particle trapping densities such as the case of single-particle trapping. Such a trapping feature whereby increased trapping stability occurs as a result of increasing particle density represents a novel form of self-induced back-action.

CONCLUSION

We have systematically studied the optical trapping process in a dielectric quasi-BIC system for the first time. We first investigate the optical trapping of dielectric subwavelength particles in a symmetry-protected quasi-BIC system that contains a pair of complete silicon elliptical cylinder resonators in each unit cell. Compared with traditional plasmonic nanotweezers, the high Q factor (~2000), strong field enhancement (~140), negligible heating effect, and multiple hotspots make such a system a great candidate for trapping-assisted sensing applications. We have also shown that purposefully truncating a small part of the tips of both resonators in each unit cell to give rise to a doubly truncated system results in an enhanced optical gradient trapping force. We attribute such enhancement to the higher electric field gradient induced in the asymmetric gap of the system. Our results show that the doubly truncated ("2 cuts") system is more suitable for particle-trapping applications in comparison to the complete elliptical nanoantenna system. In addition, we have demonstrated the positive interplay between trapped particles and the cavity in the symmetry-broken system, where only one resonator in each unit cell is truncated, in contrast to the trapping-induced suppression of the quasi-BIC modes in the original intact system. This mechanism applies to particles with lower refractive indices and smaller sizes as well. Future work will focus on experiments to demonstrate these effects. We envision that these results will pave the way for applying quasi-BIC systems into particle-trapping-assisted sensing applications and open a new door to harness the particle–cavity interplay to enhance the optical trapping process.

METHODS

Simulations. The numerical simulations of reflectance spectra and field distributions presented in here are performed by commercially available software (Lumerical FDTD Solutions 2019b) using a finite-difference time-domain solver. Periodic boundary conditions are used in the x and y directions, while PML boundary conditions are used in the z direction. A maximum mesh step of 10 nm is set for resonators, and a maximum mesh step of 3 nm is set for trapped spheres. A mesh accuracy of "5" is set for the simulation region. The dimensions, material properties, and background media are specified in the main text.

The numerical simulations of optical forces are performed by another commercially available software (COMSOL Multiphysics 5.5) using the frequency domain solver in the Wave Optics Module. Periodic boundary conditions are used in the x and y directions, while PML boundary conditions are used in the z direction. Normal-incident and x-polarized (perpendicular to the mirror plane of the unit cell) plane wave are defined at the incident port. All forces are calculated by the Maxwell stress tensor (MST) method and are all normalized to an input power of 1 mW. Material properties are averaged from the *Palik* database in Lumerical and are set as follows. $n_{Si} = 3.477$, $n_{SiO2} = 1.41$, $n_{PS} = 1.59$, and $n_{water} = 1.31 + 0.00013i$, where i is the imaginary number denoting the loss component. A maximum mesh step of 15 nm is set for resonators, and a maximum mesh step of 5 nm is set for trapped spheres. Maximum mesh steps for water and the glass substrate are set as 1550 nm/6/1.31 and 1550 nm/6/1.41, respectively. The geometrical parameters are the same as those in Lumerical simulations and are specified in the main text. It should be noted that the resonance wavelengths in COMSOL simulations all deviate slightly (~1.5 nm) from that of the same structure in Lumerical FDTD simulations. Therefore, we compare the reflection spectra and force spectra separately in the main text to avoid confusion.

https://doi.org/10.1021/acsphotonics.0c01941
ACS Photonics 2021, 8, 1961−1971

Q Factor Extraction. We use a Fano model to extract the Q factor from the reflection spectrum following the method reported in previous works.[76,77] The simulated reflection spectrum is fitted to a Fano line shape by the "CFTool" toolbox in MATLAB. The curve fitting equation is given by $R = \left| a_1 + ia_2 + \frac{b}{\omega - \omega_0 + i\gamma} \right|^2$ where a_1, a_2, and b are constant real numbers; ω_0 is estimated by the central resonant frequency and needs to be slightly modified during the fitting process; γ denotes the overall damping rate of the resonance. The frequency terms ω and ω_0 are prenormalized to (0, 1) so that all the unknown parameters will be within (0, 1). The Q factor is then calculated by $Q = (\omega_0/2\gamma)$. In this article, the R-square values of all curve fittings are larger than 99%.

■ ASSOCIATED CONTENT

Supporting Information

The Supporting Information is available free of charge at https://pubs.acs.org/doi/10.1021/acsphotonics.0c01941.

Detailed derivation for the expression of F_y; supplementary figures showing additional information such as forces on polystyrene spheres; additional proofs for the positive role of trapped particles (PDF)

■ AUTHOR INFORMATION

Corresponding Author

Justus C. Ndukaife − *Vanderbilt Institute of Nanoscale Science and Engineering and Department of Electrical Engineering and Computer Science, Vanderbilt University, Nashville, Tennessee 37235, United States;* orcid.org/0000-0002-8524-0657; Email: justus.ndukaife@vanderbilt.edu

Authors

Sen Yang − *Vanderbilt Institute of Nanoscale Science and Engineering and Interdisciplinary Materials Science, Vanderbilt University, Nashville, Tennessee 37235, United States;* orcid.org/0000-0002-0056-3052

Chuchuan Hong − *Vanderbilt Institute of Nanoscale Science and Engineering and Department of Electrical Engineering and Computer Science, Vanderbilt University, Nashville, Tennessee 37235, United States;* orcid.org/0000-0002-1329-9385

Yuxi Jiang − *Department of Electrical Engineering and Computer Science, Vanderbilt University, Nashville, Tennessee 37235, United States;* orcid.org/0000-0003-2183-1762

Complete contact information is available at: https://pubs.acs.org/10.1021/acsphotonics.0c01941

Notes

The authors declare no competing financial interest.

■ ACKNOWLEDGMENTS

The authors acknowledge financial support from the National Science Foundation (NSF ECCS-1933109) and Vanderbilt University. In addition, S.Y. would specifically like to highlight and thank the invaluable patience of Wenyi Ren. Je t'aime.

■ REFERENCES

(1) Lafratta, C. N. Optical Tweezers for Medical Diagnostics. *Anal. Bioanal. Chem.* **2013**, *405* (17), 5671−5677.

(2) Choudhary, D.; Mossa, A.; Jadhav, M.; Cecconi, C. Bio-Molecular Applications of Recent Developments in Optical Tweezers. *Biomolecules* **2019**, *9* (1), 1−19.

(3) Milic, B.; Andreasson, J. O. L.; Hogan, D. W.; Block, S. M. Intraflagellar Transport Velocity Is Governed by the Number of Active KIF17 and KIF3AB Motors and Their Motility Properties under Load. *Proc. Natl. Acad. Sci. U. S. A.* **2017**, *114* (33), E6830−E6838.

(4) Cecconi, G.; Shank, E. A.; Bustamante, C.; Marqusee, S. Biochemistry: Direct Observation of the Three-State Folding of a Single Protein Molecule. *Science (Washington, DC, U. S.)* **2005**, *309* (5743), 2057−2060.

(5) Naranjo, T.; Lemishko, K. M.; de Lorenzo, S.; Somoza, Á.; Ritort, F.; Pérez, E. M.; Ibarra, B. Dynamics of Individual Molecular Shuttles under Mechanical Force. *Nat. Commun.* **2018**, *9* (1), 1−7.

(6) Wang, S. F.; Kudo, T.; Yuyama, K. I.; Sugiyama, T.; Masuhara, H. Optically Evolved Assembly Formation in Laser Trapping of Polystyrene Nanoparticles at Solution Surface. *Langmuir* **2016**, *32* (47), 12488−12496.

(7) Kudo, T.; Wang, S. F.; Yuyama, K. I.; Masuhara, H. Optical Trapping-Formed Colloidal Assembly with Horns Extended to the Outside of a Focus through Light Propagation. *Nano Lett.* **2016**, *16* (5), 3058−3062.

(8) Ashkin, A.; Dziedzic, J. M.; Bjorkholm, J. E.; Chu, S. Observation of a Single-Beam Gradient Force Optical Trap for Dielectric Particles. *Opt. Lett.* **1986**, *11* (5), 288−290.

(9) Ashkin, A.; Dziedzic, J. M.; Yamane, T. Optical Trapping and Manipulation of Single Cells Using. *Nature* **1987**, *330*, 769−711.

(10) Ashkin, A. A.; Dziedzic, J. M. Optical Trapping and Manipulation of Viruses and Bacteria. *Science (Washington, DC, U. S.)*. **1987**, *235* (4795), 1517−1520.

(11) The Royal Swedish Academy of Sciences. Scientific Background on the Nobel Prize in Physics 2018: Groundbreaking Inventions in Laser Physics. nobelprize.org, 2018, *50005*, 1−16.

(12) Juan, M. L.; Righini, M.; Quidant, R. Plasmon Nano-Optical Tweezers. *Nat. Photonics* **2011**, *5* (6), 349−356.

(13) Ndukaife, J. C.; Kildishev, A. V.; Nnanna, A. G. A.; Shalaev, V. M.; Wereley, S. T.; Boltasseva, A. Long-Range and Rapid Transport of Individual Nano-Objects by a Hybrid Electrothermoplasmonic Nanotweezer. *Nat. Nanotechnol.* **2016**, *11* (1), 53−59.

(14) Hong, C.; Yang, S.; Ndukaife, J. C. Stand-off Trapping and Manipulation of Sub-10 Nm Objects and Biomolecules Using Opto-Thermo-Electrohydrodynamic Tweezers. *Nat. Nanotechnol.* **2020**, *15*, 908.

(15) Ndukaife, J. C.; Xuan, Y.; Nnanna, A. G. A.; Kildishev, A. V.; Shalaev, V. M.; Wereley, S. T.; Boltasseva, A. High-Resolution Large-Ensemble Nanoparticle Trapping with Multifunctional Thermoplasmonic Nanohole Metasurface. *ACS Nano* **2018**, *12* (6), 5376−5384.

(16) Juan, M. L.; Gordon, R.; Pang, Y.; Eftekhari, F.; Quidant, R. Self-Induced Back-Action Optical Trapping of Dielectric Nanoparticles. *Nat. Phys.* **2009**, *5* (12), 915−919.

(17) Saleh, A. A. E.; Dionne, J. A. Toward Efficient Optical Trapping of Sub-10-Nm Particles with Coaxial Plasmonic Apertures. *Nano Lett.* **2012**, *12* (11), 5581−5586.

(18) Yoo, D.; Gurunatha, K. L.; Choi, H. K.; Mohr, D. A.; Ertsgaard, C. T.; Gordon, R.; Oh, S. H. Low-Power Optical Trapping of Nanoparticles and Proteins with Resonant Coaxial Nanoaperture Using 10 Nm Gap. *Nano Lett.* **2018**, *18* (6), 3637−3642.

(19) Pang, Y.; Gordon, R. Optical Trapping of a Single Protein. *Nano Lett.* **2012**, *12* (1), 402−406.

(20) Kotnala, A.; Gordon, R. Quantification of High-Efficiency Trapping of Nanoparticles in a Double Nanohole Optical Tweezer. *Nano Lett.* **2014**, *14* (2), 853−856.

(21) Xu, Z.; Song, W.; Crozier, K. B. Direct Particle Tracking Observation and Brownian Dynamics Simulations of a Single Nanoparticle Optically Trapped by a Plasmonic Nanoaperture. *ACS Photonics* **2018**, *5* (7), 2850−2859.

(22) Wang, K.; Crozier, K. B. Plasmonic Trapping with a Gold Nanopillar. *ChemPhysChem* **2012**, *13* (11), 2639−2648.

(23) Zhang, W.; Huang, L.; Santschi, C.; Martin, O. J. F. Trapping and Sensing 10 Nm Metal Nanoparticles Using Plasmonic Dipole Antennas. *Nano Lett.* **2010**, *10* (3), 1006−1011.
(24) Hong, C.; Yang, S.; Ndukaife, J. C. Optofluidic Control Using Plasmonic TiN Bowtie Nanoantenna. *Opt. Mater. Express* **2019**, *9* (3), 953.
(25) Roxworthy, B. J.; Ko, K. D.; Kumar, A.; Fung, K. H.; Chow, E. K. C.; Liu, G. L.; Fang, N. X.; Toussaint, K. C. Application of Plasmonic Bowtie Nanoantenna Arrays for Optical Trapping, Stacking, and Sorting. *Nano Lett.* **2012**, *12* (2), 796−801.
(26) Berthelot, J.; Aćimović, S. S.; Juan, M. L.; Kreuzer, M. P.; Renger, J.; Quidant, R. Three-Dimensional Manipulation with Scanning near-Field Optical Nanotweezers. *Nat. Nanotechnol.* **2014**, *9* (4), 295−299.
(27) Garcés-Chávez, V.; Quidant, R.; Reece, P. J.; Badenes, G.; Torner, L.; Dholakia, K. Extended Organization of Colloidal Microparticles by Surface Plasmon Polariton Excitation. *Phys. Rev. B: Condens. Matter Mater. Phys.* **2006**, *73* (8), 1−5.
(28) Tanaka, Y.; Sasaki, K. Optical Trapping through the Localized Surface-Plasmon Resonance of Engineered Gold Nanoblock Pairs. *Opt. Express* **2011**, *19* (18), 17462.
(29) Tanaka, Y.; Sasaki, K. Efficient Optical Trapping Using Small Arrays of Plasmonic Nanoblock Pairs. *Appl. Phys. Lett.* **2012**, *100* (2), 10−13.
(30) Kotsifaki, D. G.; Truong, V. G.; Nic Chormaic, S. Dynamic Multiple Nanoparticle Trapping Using Metamaterial Plasmonic Tweezers. *Appl. Phys. Lett.* **2021**, *118* (2), 021107.
(31) Han, X.; Truong, V. G.; Chormaic, S. N. Sequential Trapping of Single Nanoparticles Using a Gold Plasmonic Nanohole Array. *Photonics Res.* **2018**, *6* (10), 981.
(32) Yu, N.; Genevet, P.; Kats, M. A.; Aieta, F.; Tetienne, J. P.; Capasso, F.; Gaburro, Z. Light Propagation with Phase Discontinuities: Generalized Laws of Reflection and Refraction. *Science (Washington, DC, U. S.)* **2011**, *334* (6054), 333−337.
(33) Kamali, S. M.; Arbabi, E.; Arbabi, A.; Faraon, A. A Review of Dielectric Optical Metasurfaces for Wavefront Control. *Nanophotonics* **2018**, *7* (6), 1041−1068.
(34) Yu, N.; Capasso, F. Flat Optics with Designer Metasurfaces. *Nat. Mater.* **2014**, *13* (2), 139−150.
(35) Arbabi, A.; Horie, Y.; Bagheri, M.; Faraon, A. Dielectric Metasurfaces for Complete Control of Phase and Polarization with Subwavelength Spatial Resolution and High Transmission. *Nat. Nanotechnol.* **2015**, *10* (11), 937−943.
(36) Yang, Y.; Wang, W.; Moitra, P.; Kravchenko, I. I.; Briggs, D. P.; Valentine, J. Dielectric Meta-Reflectarray for Broadband Linear Polarization Conversion and Optical Vortex Generation. *Nano Lett.* **2014**, *14* (3), 1394−1399.
(37) Yang, S.; Li, C.; Liu, T.; Da, H.; Feng, R.; Tang, D.; Sun, F.; Ding, W. Simple and Polarization-Independent Dammann Grating Based on All-Dielectric Nanorod Array. *J. Opt. (Bristol, U. K.)* **2017**, *19* (9), 095103.
(38) Li, Z.; Kim, M. H.; Wang, C.; Han, Z.; Shrestha, S.; Overvig, A. C.; Lu, M.; Stein, A.; Agarwal, A. M.; Lončar, M.; Yu, N. Controlling Propagation and Coupling of Waveguide Modes Using Phase-Gradient Metasurfaces. *Nat. Nanotechnol.* **2017**, *12* (7), 675−683.
(39) Liu, T.; Yang, S.; Tang, D.; Da, H.; Feng, R.; Zhu, T.; Sun, F.; Ding, W. Polarization Conversion Based on an All-Dielectric Metasurface for Optical Fiber Applications. *J. Phys. D: Appl. Phys.* **2017**, *50* (33), 334001.
(40) Nazemosadat, E.; Mazur, M.; Kruk, S.; Kravchenko, I.; Carpenter, J.; Schröder, J.; Andrekson, P. A.; Karlsson, M.; Kivshar, Y. Dielectric Broadband Metasurfaces for Fiber Mode-Multiplexed Communications. *Adv. Opt. Mater.* **2019**, *7* (14), 1−7.
(41) Chen, W. T.; Zhu, A. Y.; Sanjeev, V.; Khorasaninejad, M.; Shi, Z.; Lee, E.; Capasso, F. A Broadband Achromatic Metalens for Focusing and Imaging in the Visible. *Nat. Nanotechnol.* **2018**, *13* (3), 220−226.
(42) Capasso, F.; Khorasaninejad, M.; Chen, W. T.; Devlin, R. C.; Oh, J.; Zhu, A. Y. Metalenses at Visible Wavelengths: Diffraction-Limited Focusing and Subwavelength Resolution Imaging. *Science (Washington, DC, U. S.)* **2016**, *352* (6290), 1190−1194.
(43) von Neumann, J.; Wigner, E. Über Merkwürdige Diskrete Eigenwerte. *Phys. Z.* **1929**, *30*, 465−467 (in German).
(44) Yoon, J. W.; Song, S. H.; Magnusson, R. Critical Field Enhancement of Asymptotic Optical Bound States in the Continuum. *Sci. Rep.* **2015**, *5*, 1−8.
(45) Sadrieva, Z. F.; Sinev, I. S.; Koshelev, K. L.; Samusev, A.; Iorsh, I. V.; Takayama, O.; Malureanu, R.; Bogdanov, A. A.; Lavrinenko, A. V. Transition from Optical Bound States in the Continuum to Leaky Resonances: Role of Substrate and Roughness. *ACS Photonics* **2017**, *4* (4), 723−727.
(46) Choi, D.-Y.; Kivshar, Y. S.; Neshev, D. N.; Liu, M.; Altug, H.; Tittl, A.; Yesilkoy, F.; Leitis, A. Imaging-Based Molecular Barcoding with Pixelated Dielectric Metasurfaces. *Science (Washington, DC, U. S.)* **2018**, *360* (6393), 1105−1109.
(47) Yesilkoy, F.; Arvelo, E. R.; Jahani, Y.; Liu, M.; Tittl, A.; Cevher, V.; Kivshar, Y.; Altug, H. Ultrasensitive Hyperspectral Imaging and Biodetection Enabled by Dielectric Metasurfaces. *Nat. Photonics* **2019**, *13* (6), 390−396.
(48) Ndao, A.; Hsu, L.; Cai, W.; Ha, J.; Park, J.; Contractor, R.; Lo, Y.; Kanté, B. Differentiating and Quantifying Exosome Secretion from a Single Cell Using Quasi-Bound States in the Continuum. *Nanophotonics* **2020**, *9*, 1081.
(49) Koshelev, K.; Kruk, S.; Melik-Gaykazyan, E.; Choi, J. H.; Bogdanov, A.; Park, H. G.; Kivshar, Y. Subwavelength Dielectric Resonators for Nonlinear Nanophotonics. *Science (Washington, DC, U. S.)* **2020**, *367* (6475), 288−292.
(50) Carletti, L.; Koshelev, K.; De Angelis, C.; Kivshar, Y. Giant Nonlinear Response at the Nanoscale Driven by Bound States in the Continuum. *Phys. Rev. Lett.* **2018**, *121* (3), 33903.
(51) Koshelev, K.; Tang, Y.; Li, K.; Choi, D. Y.; Li, G.; Kivshar, Y. Nonlinear Metasurfaces Governed by Bound States in the Continuum. *ACS Photonics* **2019**, *6* (7), 1639−1644.
(52) Koshelev, K.; Jahani, Y.; Tittl, A.; Altug, H.; Kivshar, Y. Enhanced Circular Dichroism and Chiral Sensing with Bound States in the Continuum. *2019 Conf. Lasers Electro-Optics, CLEO 2019 - Proc.* **2019**, 4−5.
(53) Yin, X.; Jin, J.; Soljačić, M.; Peng, C.; Zhen, B. Observation of Topologically Enabled Unidirectional Guided Resonances. *Nature* **2020**, *580* (7804), 467−471.
(54) Kodigala, A.; Lepetit, T.; Gu, Q.; Bahari, B.; Fainman, Y.; Kanté, B. Lasing Action from Photonic Bound States in Continuum. *Nature* **2017**, *541* (7636), 196−199.
(55) Hsu, C. W.; Zhen, B.; Stone, A. D.; Joannopoulos, J. D.; Soljacic, M. Bound States in the Continuum. *Nat. Rev. Mater.* **2016**, *1* (9), No. 16048.
(56) Koshelev, K.; Lepeshov, S.; Liu, M.; Bogdanov, A.; Kivshar, Y. Asymmetric Metasurfaces with High- Q Resonances Governed by Bound States in the Continuum. *Phys. Rev. Lett.* **2018**, *121* (19), 193903.
(57) Koshelev, K.; Bogdanov, A.; Kivshar, Y. Meta-Optics and Bound States in the Continuum. *Sci. Bull.* **2019**, *64* (12), 836−842.
(58) Lee, J.; Zhen, B.; Chua, S. L.; Qiu, W.; Joannopoulos, J. D.; Soljačić, M.; Shapira, O. Observation and Differentiation of Unique High-Q Optical Resonances near Zero Wave Vector in Macroscopic Photonic Crystal Slabs. *Phys. Rev. Lett.* **2012**, *109* (6), 1−5.
(59) Plotnik, Y.; Peleg, O.; Dreisow, F.; Heinrich, M.; Nolte, S.; Szameit, A.; Segev, M. Experimental Observation of Optical Bound States in the Continuum. *Phys. Rev. Lett.* **2011**, *107* (18), 28−31.
(60) Xu, Z.; Song, W.; Crozier, K. B. Optical Trapping of Nanoparticles Using All-Silicon Nanoantennas. *ACS Photonics* **2018**, *5* (12), 4993−5001.
(61) Joannopoulos, J. D.; Johnson, S. G.; Winn, J. N.; Meade, R. D. *Photonic Crystals: Molding the Flow of Light*, 2nd ed.; Princeton University Press, 2011.
(62) Hu, S.; Khater, M.; Salas-Montiel, R.; Kratschmer, E.; Engelmann, S.; Green, W. M. J.; Weiss, S. M. Experimental

Realization of Deep-Subwavelength Confinement in Dielectric Optical Resonators. *Sci. Adv.* **2018**, *4* (8), eaat2355.
(63) Hu, S.; Weiss, S. M. Design of Photonic Crystal Cavities for Extreme Light Concentration. *ACS Photonics* **2016**, *3* (9), 1647−1653.
(64) Kwak, E. S.; Onuta, T. D.; Amarie, D.; Potyrailo, R.; Stein, B.; Jacobson, S. C.; Schaich, W. L.; Dragnea, B. Optical Trapping with Integrated Near-Field Apertures. *J. Phys. Chem. B* **2004**, *108* (36), 13607−13612.
(65) Chen, C.; Juan, M. L.; Li, Y.; Maes, G.; Borghs, G.; Van Dorpe, P.; Quidant, R. Enhanced Optical Trapping and Arrangement of Nano-Objects in a Plasmonic Nanocavity. *Nano Lett.* **2012**, *12* (1), 125−132.
(66) Pang, Y.; Gordon, R. Optical Trapping of 12 Nm Dielectric Spheres Using Double-Nanoholes in a Gold Film. *Nano Lett.* **2011**, *11* (9), 3763−3767.
(67) Mestres, P.; Berthelot, J.; Acimovic, S. S.; Quidant, R. Unraveling the Optomechanical Nature of Plasmonic Trapping. *Light: Sci. Appl.* **2016**, *5* (7), 1−6.
(68) Zhu, T.; Cao, Y.; Wang, L.; Nie, Z.; Cao, T.; Sun, F.; Jiang, Z.; Nieto-Vesperinas, M.; Liu, Y.; Qiu, C. W.; Ding, W. Self-Induced Backaction Optical Pulling Force. *Phys. Rev. Lett.* **2018**, *120* (12), 1−6.
(69) Descharmes, N.; Dharanipathy, U. P.; Diao, Z.; Tonin, M.; Houdré, R. Observation of Backaction and Self-Induced Trapping in a Planar Hollow Photonic Crystal Cavity. *Phys. Rev. Lett.* **2013**, *110* (12), 1−4.
(70) Neumeier, L.; Quidant, R.; Chang, D. E. Self-Induced Back-Action Optical Trapping in Nanophotonic Systems. *New J. Phys.* **2015**, *17* (12), 123008.
(71) Grahn, P.; Shevchenko, A.; Kaivola, M. Electromagnetic Multipole Theory for Optical Nanomaterials. *New J. Phys.* **2012**, *14*, 093033.
(72) Aspelmeyer, M.; Kippenberg, T. J.; Marquardt, F. Cavity Optomechanics. *Rev. Mod. Phys.* **2014**, *86* (4), 1391−1452.
(73) Saleh, A. A. E.; Dionne, J. A. Toward Efficient Optical Trapping of Sub-10-Nm Particles with Coaxial Plasmonic Apertures. *Nano Lett.* **2012**, *12* (11), 5581−5586.
(74) Leng, H.; Szychowski, B.; Daniel, M. C.; Pelton, M. Strong Coupling and Induced Transparency at Room Temperature with Single Quantum Dots and Gap Plasmons. *Nat. Commun.* **2018**, *9* (1), No. 4012.
(75) Rodrigo, D.; Limaj, O.; Janner, D.; Etezadi, D.; García De Abajo, F. J.; Pruneri, V.; Altug, H. Mid-Infrared Plasmonic Biosensing with Graphene. *Science (Washington, DC, U. S.)* **2015**, *349* (6244), 165−168.
(76) Wu, C.; Arju, N.; Kelp, G.; Fan, J. A.; Dominguez, J.; Gonzales, E.; Tutuc, E.; Brener, I.; Shvets, G. Spectrally Selective Chiral Silicon Metasurfaces Based on Infrared Fano Resonances. *Nat. Commun.* **2014**, *5* (May), 1−9.
(77) Yang, Y.; Kravchenko, I. I.; Briggs, D. P.; Valentine, J. All-Dielectric Metasurface Analogue of Electromagnetically Induced Transparency. *Nat. Commun.* **2014**, *5*, 1−7.

https://doi.org/10.1021/acsphotonics.0c01941
ACS Photonics 2021, 8, 1961−1971